Mechanics of Materials 83 (2015) 122–135

Contents lists available at ScienceDirect

Mechanics of Materials

journal homepage: www.elsevier.com/locate/mechmat

Generalized shear of a bilayer

Dong Wang, M.S. Wu *

School of Mechanical and Aerospace Engineering, Nanyang Technological University, Singapore 639798

ARTICLE INFO

Article history:
Received 19 August 2014
Received in revised form 22 December 2014
Available online 12 January 2015

Keywords:
Bilayer block
Generalized shear
Poynting effect
Sinusoidal shear stress

ABSTRACT

A bilayer block with dissimilar elastic constants under generalized shear is studied. The shear displacement is not constrained *a priori* to be a function of the vertical coordinate. Using second-order isotropic elasticity and under a prescribed shear displacement on the top face, the shear displacement takes the form of the product of sine and hyperbolic sine functions. There exist first- and second-order shear stresses, as well as second-order normal stresses corresponding to the Poynting effect. The shear moduli inhomogeneity between the layers has an "intrinsic" influence on the second-order normal stresses, meaning that this influence persists even if both shear moduli approach zero. Generally, the elastic inhomogeneity has a strong influence on the sign, magnitude and functional variation of the stresses and displacements. A generalized Poynting effect, associated with a sinusoidal shear stress, is also predicted in which the sheared block distorts not only in plane but also tends to distort out of plane. Experimental results on the deformed lateral profiles of agar–gelatin bilayers show reasonable agreement with theory.

1. Introduction

The simple shear of soft solids under finite deformation has been investigated in a number of recent works, e.g., Destrade and Saccomandi (2010), Horgan and Murphy (2011), Destrade et al. (2012) and Mihai and Goriely (2013). The importance of nonlinear phenomena such as the development of normal stresses under simple shear, which corresponds to the Poynting effect in which a cylinder under torsion elongates or shortens in length, has been highlighted. Interestingly, Storm et al. (2005), Janmey et al. (2007) and Kang et al. (2009) have reported negative normal stresses in biological gels, i.e., the sheared faces of the block tend to be drawn towards each other. Wu and Kirchner (2010) and Wang and Wu (2014a) have studied the dependence of these nonlinear phenomena on elastic constants in torsion problems using second-order elasticity. The effect of dissimilar elastic constants in a bilayer cylinder has been emphasized in the latter work.

Much of the recent efforts have focused on homogeneous solids. However, bilayer systems under shear constitute an important class of problems. Many natural and synthetic material systems consist of two or more layers with different mechanical, chemical and other properties. Examples, to name a few, include skins, muscles, artificial tissue constructs, lipid bilayers, graphene bilayers, multilayer substrates for stem cell cultivation, and bio-inspired devices. The study of lipid bilayers under mechanical forces remains of considerable interest. Butler et al. (2001) studied the influence of shear on the lateral diffusion of endothelial cell membrane lipids. Jönsson et al. (2009) investigated the mechanical behavior of lipid bilayers in microfluidic channels under shear forces. Peng et al. (2013) developed computational models for lipid bilayers attached to the spectrin cytoskeletal network of red blood cell membranes. Furthermore, much interest has recently developed in graphene, which demonstrate nonlinear elasticity (Lu and Huang, 2009; Cadelano et al., 2009). Apparently the mechanical behavior of graphene bilayers is also rapidly gaining attention (Scarpa et al., 2010).

* Corresponding author. Tel.: +65 6790 5545.
E-mail address: mmswu@ntu.edu.sg (M.S. Wu).

http://dx.doi.org/10.1016/j.mechmat.2015.01.003
0167-6636/

In this work, we consider the basic problem of a bilayer solid subjected to generalized shear in the framework of second-order elasticity. A uniform shear displacement is imposed at the top of the bilayer, whose bottom is held fixed. The shear is generalized in the sense that *a priori* assumption has not been made regarding the dependence of the shear displacement versus the vertical coordinate (along the height direction) of the block. The deformation takes the form: $x = X + U(Y, Z)$, $y = Y + V(Y)$, $z = Z$, where x, y, z and X, Y, Z denote coordinates in the deformed and reference configurations, respectively, and U, V the displacements. The current study is based on the earlier work for a homogeneous soft block (Wang and Wu, 2014b). The new contribution consists of the study of the dependence of (i) the induced normal stresses and shear stresses, and (ii) the interfacial stresses and displacements, on the dissimilar sets of elastic constants, as well as experimental verification of the predicted variation of the shear displacement with the vertical coordinate.

Following this introduction, we present the formulation, numerical/experimental results, and conclusions in four sections.

2. Second-order formulation of the generalized shear of a bilayer

2.1. Definition of problem

We consider a bilayer rectangular block under generalized shear as shown in Fig 1. Each layer is homogeneous and isotropic. Denote X, Y, Z as the reference coordinates, with X along the direction of the imposed shear, Y along the height and Z along the depth. The lengths of the block in the X and Z directions are denoted by L_X and L_Z, respectively, while the thicknesses of the bottom (first) and top (second) layers are denoted by $L_Y^{(1)}$ and $L_Y^{(2)}$, respectively. Let also $L_Y = L_Y^{(1)} + L_Y^{(2)}$. The deformed coordinates are assumed to be $(X + U^{(i)}, Y + V^{(i)}, Z)$, with $i = 1, 2$ for the layers. Here, $U^{(i)} = u_1^{(i)}(Y, Z) + k u_2^{(i)}(Y, Z)$ denotes the shear displacement in the X-direction for the ith layer, with $u_1^{(i)}$ and $u_2^{(i)}$ representing the linear and nonlinear components, respectively. $U^{(i)}$ is taken to be a function of both Y and Z, allowing for the possibility of a non-uniform (generalized) shear. No assumption is made regarding the dependence of $U^{(i)}$ on Y or Z, as it will be solved from the equilibrium equations; this differs from the simple shear mode in which $U^{(i)}$ is assumed to be linearly dependent on Y only. Similarly, $V^{(i)} = v_1^{(i)}(Y) + k v_2^{(i)}(Y)$ denotes the displacement in the Y-direction, with $v_1^{(i)}$ and $v_2^{(i)}$ denoting the linear and nonlinear components. Note that $V^{(i)}$ is taken to be solely a function of Y. Gravity effect is neglected. Also, k is a marker indicating the order of approximation of the theory. In the subsequent formulation, we retain terms up to k^2 for the second-order theory.

2.2. Governing equations

2.2.1. Second-order elasticity model

The differentials of position vectors in the undeformed state are:

$$\begin{pmatrix} dX \\ dY \\ dZ \end{pmatrix}, \tag{2.1}$$

while in the deformed state they are:

$$\begin{pmatrix} dX + k\left(\frac{\partial u_1^{(i)}}{\partial Y} dY + \frac{\partial u_1^{(i)}}{\partial Z} dZ\right) + k^2\left(\frac{\partial u_2^{(i)}}{\partial Y} dY + \frac{\partial u_2^{(i)}}{\partial Z} dZ\right) \\ dY + k\, dv_1^{(i)} + k^2 dv_2^{(i)} \\ dZ \end{pmatrix}, \tag{2.2}$$

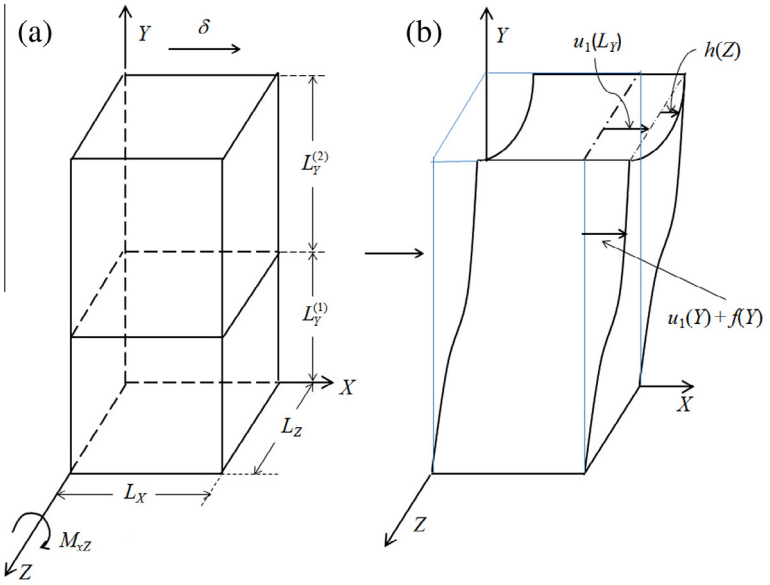

Fig. 1. (a) A bilayered rectangular block of dimensions L_X, $L_Y^{(1)} + L_Y^{(2)}$ and L_Z in the undeformed state. (b) The block deformed under generalized shear. The prescribed displacement at the top face $Y = L_Y$ consists of the linear part $u_1(L_Y)$ and the nonlinear part $u_2(Y = L_Y, Z) = h(Z)$. The problem of $h(Z) = 0$ is considered for simplicity. The lateral profile of the block, or the deformed shaped of the four vertical edges of the box, is written as $u_1(Y) + f(Y)$.

for $i = 1, 2$ respectively. Based on Eq. (2.2), the deformation gradient $\mathbf{F}$ can be written as:

$$\mathbf{F} = \begin{pmatrix} 1 & k\frac{\partial u_1^{(i)}}{\partial Y} + k^2\frac{\partial u_2^{(i)}}{\partial Y} & k\frac{\partial u_1^{(i)}}{\partial Z} + k^2\frac{\partial u_2^{(i)}}{\partial Z} \\ 0 & 1 + k\frac{dv_1^{(i)}}{dY} + k^2\frac{dv_2^{(i)}}{dY} & 0 \\ 0 & 0 & 1 \end{pmatrix}. \tag{2.3}$$

In this formulation, $\mathbf{F}$ contains an additional term $k\left(\partial u_1^{(i)}/\partial Z\right) + k^2\left(\partial u_2^{(i)}/\partial Z\right)$, which exists because $U^{(i)}$ is a function of both Y and Z.

The energy density W of Murnaghan (1951) is:

$$W = \frac{\lambda + 2\mu}{2}J_1^2 - 2\mu J_2 + \frac{l + 2m}{3}J_1^3 - 2mJ_1J_2 + nJ_3, \tag{2.4}$$

where λ and μ are the second-order and l, m, n the third-order elastic constants, respectively, and J_1, J_2, and J_3 are the strain invariants of the Lagrangian strain $\mathbf{E}$:

$$J_1 = E_1 + E_2 + E_3,\ J_2 = E_1E_2 + E_2E_3 + E_3E_1,\ J_3 = E_1E_2E_3, \tag{2.5}$$

with E_1, E_2 and E_3 denoting the principal values. The Lagrangian strain is expressed in terms of the deformation gradient as:

$$\mathbf{E} = \frac{1}{2}(\mathbf{F}^*\mathbf{F} - \mathbf{I}), \tag{2.6}$$

where $\mathbf{I}$ is the identity and the asterisk denotes the transpose. The first Piola–Kirchhoff stress (relating forces in the current configuration to area vectors in the undeformed configuration, and generally non-symmetric) is defined as:

$$\begin{aligned}\mathbf{T} &= \mathbf{F}\frac{\partial W}{\partial \mathbf{E}} \\ &= \mathbf{F}\left(\lambda J_1\mathbf{I} + 2\mu\mathbf{E} + (lJ_1^2 - 2mJ_2)\mathbf{I} + 2mJ_1\mathbf{E} + n\,\mathrm{co}\,\mathbf{E}\right),\end{aligned} \tag{2.7}$$

where co $\mathbf{E}$ is the cofactor matrix.

2.2.2. Equilibrium Equations

The Lagrangian equilibrium equations in Cartesian coordinates can be written as:

$$\begin{aligned}&\frac{\partial T_{xX}}{\partial X} + \frac{\partial T_{xY}}{\partial Y} + \frac{\partial T_{xZ}}{\partial Z} = 0,\\ &\frac{\partial T_{yX}}{\partial X} + \frac{\partial T_{yY}}{\partial Y} + \frac{\partial T_{yZ}}{\partial Z} = 0,\\ &\frac{\partial T_{zX}}{\partial X} + \frac{\partial T_{zY}}{\partial Y} + \frac{\partial T_{zZ}}{\partial Z} = 0,\end{aligned} \tag{2.8}$$

In the notation for the stress component such as T_{xX}, the first subscript in lower case denotes the stress direction in the current configuration and the second subscript in upper case denotes the unit vector direction of the element surface in the reference configuration. Substituting the stresses from Eq. (2.7) into Eq. (2.8) yields the following two first-order (k) and four second-order (k^2) equations for each layer:

$$k\mu\left(\frac{\partial^2 u_1^{(i)}}{\partial Y^2} + \frac{\partial^2 u_1^{(i)}}{\partial Z^2}\right) = 0, \tag{2.9}$$

$$k^2\mu\left(\frac{\partial^2 u_2^{(i)}}{\partial Y^2} + \frac{\partial^2 u_2^{(i)}}{\partial Z^2}\right) = 0, \tag{2.10}$$

$$\begin{aligned}&\frac{1}{4}k^2\Bigg((4\lambda + 4\mu + 4m - n)\frac{\partial u_1^{(i)}}{\partial Z}\frac{\partial^2 u_1^{(i)}}{\partial Y\partial Z}\\ &\quad + 4(\lambda + 2\mu + m)\frac{\partial u_1^{(i)}}{\partial Y}\frac{\partial^2 u_1^{(i)}}{\partial Y^2} + (4\mu + n)\frac{\partial u_1^{(i)}}{\partial Y}\frac{\partial^2 u_1^{(i)}}{\partial Z^2}\Bigg) = 0,\end{aligned} \tag{2.11}$$

$$\begin{aligned}&\frac{1}{4}k^2\Bigg((4\lambda + 4\mu + 4m - n)\frac{\partial u_1^{(i)}}{\partial Y}\frac{\partial^2 u_1^{(i)}}{\partial Y\partial Z}\\ &\quad + 4(\lambda + 2\mu + m)\frac{\partial u_1^{(i)}}{\partial Z}\frac{\partial^2 u_1^{(i)}}{\partial Z^2} + (4\mu + n)\frac{\partial^2 u_1^{(i)}}{\partial Y^2}\frac{\partial u_1^{(i)}}{\partial Z}\Bigg) = 0,\end{aligned} \tag{2.12}$$

$$kv_1^{(i)\prime\prime}(Y) = 0, \tag{2.13}$$

$$k^2 v_2^{(i)\prime\prime}(Y) = 0. \tag{2.14}$$

The first two are Laplace equations, and the last two are second-order linear ordinary differential equations. The middle two are partial differential equations with mixed derivatives. These equations can be solved by applying appropriate boundary conditions.

2.3. General solutions

The basic boundary conditions applied to the block are: (1) the bottom of the block is fixed, (2) an applied linear displacement δ_2 is applied to the top face of the block, (3) the total height of the block is maintained, and (4) a restraining moment preventing the block from rotating about the Z-axis. This restraining moment is generally non-vanishing and arises from a second-order effect due to the existence of T_{xZ} (shown later). It is denoted by M_{xZ} in association with T_{xZ}. Other conditions are the continuity of displacements and tractions across the interface, and no net shear forces are applied on the Z-faces. The objective is to obtain solutions for the displacements $U^{(i)} = u_1^{(i)}(Y,Z) + ku_2^{(i)}(Y,Z)$ and $V^{(i)} = v_1^{(i)}(Y) + kv_2^{(i)}(Y)$ in the two layers. The details are given in the Sections 2.3.1, 2.3.2, 2.3.3 below, in which $v_1^{(i)}(Y)$ and $v_2^{(i)}(Y)$ are obtained in Section 2.3.1, $u_1^{(i)}(Y,Z)$ in Section 2.3.2, and finally $u_2^{(i)}(Y,Z)$ in Section 2.3.3.

2.3.1. Vertical linear and nonlinear displacements

The linear and nonlinear Y-direction displacements v_1 and v_2 can be solved from Eqs. (2.13) and (2.14) as:

$$\begin{aligned}&v_1^{(1)} = C_1^{(1)}Y + C_2^{(1)},\ v_1^{(2)} = C_1^{(2)}Y + C_2^{(2)},\\ &v_2^{(1)} = C_3^{(1)}Y + C_4^{(1)},\ v_2^{(2)} = C_3^{(2)}Y + C_4^{(2)}.\end{aligned} \tag{2.15}$$

Both $v_1^{(i)}$ and $v_2^{(i)}$ are linear functions of the Ycoordinate, with eight unknowns $C_1^{(1)}$, $C_2^{(1)}$, $C_3^{(1)}$, $C_4^{(1)}$ and $C_1^{(2)}$, $C_2^{(2)}$, $C_3^{(2)}$, $C_4^{(2)}$. The following boundary conditions are applied to determine the eight unknowns:

(BC1) The bottom is fixed, i.e., there is no vertical displacement at $Y = 0$,

(BC2) The total height is maintained,
(BC3) Both the linear and nonlinear displacements are continuous at the interface $Y = L_Y^{(1)}$,
(BC4) Both the linear and nonlinear stresses T_{yY}^{L} and T_{yY}^{NL} are continuous across the interface $Y = L_Y^{(1)}$.

The expressions for the stresses required in (BC4) can be obtained via Eq. (2.7). Mathematically, the above boundary conditions can be written as:

$$\text{(BC1)}\ v_1^{(1)}(Y=0)=0 \text{ and } v_2^{(1)}(Y=0)=0, \tag{2.16}$$

$$\text{(BC2)}\ v_1^{(2)}(Y=L_Y^{(1)}+L_Y^{(2)})=0 \text{ and } v_2^{(2)}(Y=L_Y^{(1)}+L_Y^{(2)})=0, \tag{2.17}$$

$$\text{(BC3)}\ v_1^{(1)}(Y=L_Y^{(1)})=v_1^{(2)}(Y=L_Y^{(1)}) \text{ and } v_2^{(1)}(Y=L_Y^{(1)})=v_2^{(2)}(Y=L_Y^{(1)}), \tag{2.18}$$

$$\text{(BC4)}\ T_{yY}^{(1)L}(Y=L_Y^{(1)})=T_{yY}^{(2)L}(Y=L_Y^{(1)}) \text{ and } T_{yY}^{(1)NL}(Y=L_Y^{(1)})=T_{yY}^{(2)NL}(Y=L_Y^{(1)}). \tag{2.19}$$

Use the above 8 equations, the eight unknowns in Eq. (2.15) can be solved as:

$$\begin{aligned}
&C_1^{(1)}=0,\ C_2^{(1)}=0,\ C_1^{(2)}=0,\ C_2^{(2)}=0,\\
&C_3^{(1)}=\frac{-m_1\alpha_1^2+m_2\alpha_2^2-\alpha_1^2\lambda_1+\alpha_2^2\lambda_2-2\alpha_1^2\mu_1+2\alpha_2^2\mu_2}{2\left(L_Y^{(2)}(\lambda_1+2\mu_1)+L_Y^{(1)}(\lambda_2+2\mu_2)\right)}L_Y^{(2)},\\
&C_4^{(1)}=0,\\
&C_3^{(2)}=\frac{m_1\alpha_1^2-m_2\alpha_2^2+\alpha_1^2\lambda_1-\alpha_2^2\lambda_2+2\alpha_1^2\mu_1-2\alpha_2^2\mu_2}{2\left(L_Y^{(2)}(\lambda_1+2\mu_1)+L_Y^{(1)}(\lambda_2+2\mu_2)\right)}L_Y^{(1)},\\
&C_4^{(2)}=\frac{-m_1\alpha_1^2+m_2\alpha_2^2-\alpha_1^2\lambda_1+\alpha_2^2\lambda_2-2\alpha_1^2\mu_1+2\alpha_2^2\mu_2}{2\left(L_Y^{(2)}(\lambda_1+2\mu_1)+L_Y^{(1)}(\lambda_2+2\mu_2)\right)}L_Y^{(1)}(L_Y^{(1)}+L_Y^{(2)}),
\end{aligned} \tag{2.20}$$

where α_1 and α_2 are the linear shear strains carried by the lower and upper blocks, respectively. These linear shear strains enter Eq. (2.20) through the dependence of $T_{yY}^{(i)NL}$ on α_1 and α_2, whose explicit forms will be obtained in the next sub-section. Note that only three constants associated with the second-order effects are non-zero, and all eight constants are zero if the bilayer block reduces to a homogeneous one. Hence, second-order vertical displacements in the block arise because of the elastic dissimilarity.

2.3.2. Linear shear displacements

The linear shear displacement $u_1^{(i)}$ can be solved from Eqs. (2.9), (2.11) and (2.12), yielding:

$$u_1^{(1)}=\alpha_1 Y+\beta_1, \quad u_1^{(2)}=\alpha_2 Y+\beta_2. \tag{2.21}$$

There are totally four unknowns: α_1, α_2, β_1 and β_2. These solutions represent the simple shear for a bilayered block in the first-order theory. The following force and displacement boundary conditions in the X-direction (resulting in four equations) are applied:

(BC1) The imposed shear displacement at the top face is δ_2, or equivalently linear shear forces F_1 are applied at the top and bottom faces,
(BC2) The bottom face is fixed,
(BC3) The linear shear displacement is continuous at the interface.

Mathematically, they can be written as:

$$\text{(BC1)}\ \alpha_1\mu_1 L_X L_Z=F_1 \text{ and } \alpha_2\mu_2 L_X L_Z=F_1, \tag{2.22}$$

$$\text{(BC2)}\ u_1^{(1)}(Y=0)=0, \tag{2.23}$$

$$\text{(BC3)}\ u_1^{(1)}(Y=L_Y^{(1)})=u_1^{(2)}(Y=L_Y^{(1)}). \tag{2.24}$$

In Eq. (2.22), $\alpha_1=\delta_1/L_Y^{(1)}$, $\alpha_2=(\delta_2-\delta_1)/L_Y^{(2)}$, where δ_1 is the shear displacement (in the X-direction) of the interface. Eq. (2.22) essentially means that the linear shear stress $T_{xY}^{L}=k\alpha_i\mu_i$ is constant in both layers, i.e., $\alpha_1\mu_1=\alpha_2\mu_2$, with $\alpha_1\neq\alpha_2$ generally. Using these four equations, α_1, α_2, β_1, β_2 are solved in terms of F_1 or δ_2 as:

$$\begin{aligned}
&\alpha_1=\frac{F_1}{\mu_1 L_X L_Z}=\frac{\delta_2}{L_Y^{(1)}+(\mu_1/\mu_2)L_Y^{(2)}},\\
&\alpha_2=\frac{F_1}{\mu_2 L_X L_Z}=\frac{\delta_2}{(\mu_2/\mu_1)L_Y^{(1)}+L_Y^{(2)}},\\
&\beta_1=0, \quad \beta_2=\frac{F_1(\mu_2-\mu_1)L_Y^{(1)}}{\mu_1\mu_2 L_X L_Z}.
\end{aligned} \tag{2.25}$$

The coefficients $C_3^{(1)}$, $C_3^{(2)}$ and $C_4^{(2)}$ in Eq. (2.20) are thus explicitly obtained. As expected, $\alpha_1=\alpha_2$ and $\beta_1=\beta_2=0$ for a homogeneous block.

2.3.3. Nonlinear shear displacements

The nonlinear shear displacements $u_2^{(i)}$ are solved next. To do this, first write down the matrix of the first Piola–Kirchhoff stress using Eq. (2.7), i.e.:

$$\begin{bmatrix}
\frac{1}{2}k^2\left(2C_3^{(i)}\lambda+\alpha_i^2(m_i+\lambda_i+2\mu_i)\right) & k\alpha_i\mu_i+k^2\mu_i\frac{\partial u_2^{(i)}}{\partial Y} & k^2\mu_i\frac{\partial u_2^{(i)}}{\partial Y}\\
k\alpha_i\mu_i+k^2\mu_i\frac{\partial u_2^{(i)}}{\partial Y} & \frac{1}{2}k^2\left(m_i\alpha_i^2+\left(2C_3^{(i)}+\alpha_i^2\right)(\lambda_i+2\mu_i)\right) & 0\\
k^2\mu_i\frac{\partial u_2^{(i)}}{\partial Y} & 0 & \frac{1}{4}k^2\left(2m_i\alpha_i^2-n_i\alpha_i^2+4\lambda_i C_3^{(i)}+2\lambda_i\alpha_i^2\right)
\end{bmatrix}, \tag{2.26}$$

where $C_3^{(i)}$ and α_i are given in Eqs. (2.20) and (2.25), respectively. This stress matrix is symmetric. All the normal stresses T_{xX}, T_{yY}, T_{zZ} and the shear stress T_{xZ} are second-order whereas the shear stress T_{xY} consists of both first- and second-order parts. Two important points are highlighted here. First, T_{xZ} being related to the derivative of the nonlinear shear displacement $u_2(Y,Z)$ with respect to Y, is generally non-zero. Summing the moments of the elementary shear forces $T_{xZ}\,dXdZ$ about the X- and Y-axis leads to zero automatically, but to a non-vanishing moment M_{xZ} about the Z-axis. Hence, to maintain the block according to the imposed deformation, a restraining moment M_{xZ} is necessary. In the experiments, this is imposed by providing constraints to the top and bottom faces to prevent it from undergoing any net rotation. Second, the second-order stress $T_{xZ} = T_{zX}$ is not present in simple shear, in contrast to the second-order normal stresses (which correspond to the Poynting effect). Thus, for the generalized shear considered here, out-of-plane shear stresses in addition to normal stresses are induced.

The governing equation for $u_2^{(i)}$ is the Laplace equation, Eq. (2.10). The displacement boundary conditions on the top and bottom ($Y = 0,\ L_Y^{(1)} + L_Y^{(2)}$) faces are applied first:

(BC1)

$$u_2(Y=0,Z)=0, \tag{2.27}$$

(BC2)

$$h(Z)=u_2\left(Y=L_Y^{(1)}+L_Y^{(2)},Z\right), \tag{2.28}$$

i.e., the bottom face is fixed and $h(Z)$ is the nonlinear shear displacement prescribed at the top $Y = L_Y^{(1)} + L_Y^{(1)}$. We note that the ratio of the imposed linear to nonlinear displacements is not known *a priori*. In the particular problem to be considered, $h(Z)$ will be set to the simplest choice of zero and the predicted shape of the block is compared to experimental results. Furthermore, we define:

$$u_2(Y,Z=L_Z)=u_2(Y,Z=0)=f(Y), \tag{2.29}$$

$$u_2\left(Y=L_Y^{(1)},Z\right)=g(Z), \tag{2.30}$$

where $f(Y)$ is the nonlinear deformation of the block at $Z = 0$ and $Z = L_Z$, respectively. The shape $f(Y)$, which we will call the lateral profile, illustrates how the block deflects laterally in the XY plane. Also, $g(Z)$ is the nonlinear shear deformation of the block at the interface $Y = L_Y^{(1)}$. The second-order displacement u_2 can then be obtained for both the first and second layers, as explained next.

For the first or bottom layer, solving Eq. (2.10) leads to:

$$\begin{aligned}u_2^{(1)}(Y,Z)=&\sum_{n=1}^{\infty}A_n^{(1)}\sin\left(\frac{n\pi Y}{L_Y^{(1)}}\right)\sinh\left(\frac{n\pi(L_Z-Z)}{L_Y^{(1)}}\right)\\&+\sum_{n=1}^{\infty}B_n^{(1)}\sin\left(\frac{n\pi Y}{L_Y^{(1)}}\right)\sinh\left(\frac{n\pi Z}{L_Y^{(1)}}\right)\\&+\sum_{n=1}^{\infty}D_n^{(1)}\sinh\left(\frac{n\pi Y}{L_Z}\right)\sin\left(\frac{n\pi Z}{L_Z}\right),\end{aligned} \tag{2.31}$$

where the coefficients

$$\begin{aligned}A_n^{(1)}&=B_n^{(1)}\\&=\frac{2}{L_Y^{(1)}\sinh\left(\frac{n\pi L_Z}{L_Y^{(1)}}\right)}\int_0^{L_Y^{(1)}}f(Y)\sin\left(\frac{n\pi Y}{L_Y^{(1)}}\right)dY,\end{aligned} \tag{2.32}$$

and

$$D_n^{(1)}=\frac{2}{L_Z\sinh\left(\frac{n\pi L_Y^{(1)}}{L_Z}\right)}\int_0^{L_Z}g(Z)\sin\left(\frac{n\pi Z}{L_Z}\right)dZ. \tag{2.33}$$

For the second or top layer:

$$\begin{aligned}u_2^{(2)}(Y,Z)=&\sum_{n=1}^{\infty}A_n^{(2)}\sin\left(\frac{n\pi(Y-L_Y^{(1)})}{L_Y^{(2)}}\right)\sinh\left(\frac{n\pi(L_Z-Z)}{L_Y^{(2)}}\right)\\&+\sum_{n=1}^{\infty}B_n^{(2)}\sin\left(\frac{n\pi(Y-L_Y^{(1)})}{L_Y^{(2)}}\right)\sinh\left(\frac{n\pi Z}{L_Y^{(2)}}\right)\\&+\sum_{n=1}^{\infty}C_n^{(2)}\sinh\left(\frac{n\pi(L_Y^{(1)}+L_Y^{(2)}-Y)}{L_Z}\right)\sin\left(\frac{n\pi Z}{L_Z}\right)\\&+\sum_{n=1}^{\infty}D_n^{(2)}\sinh\left(\frac{n\pi(Y-L_Y^{(1)})}{L_Z}\right)\sin\left(\frac{n\pi Z}{L_Z}\right),\end{aligned} \tag{2.34}$$

where

$$\begin{aligned}A_n^{(2)}=B_n^{(2)}=&\frac{2}{L_Y^{(2)}\sinh\left(\frac{n\pi L_Z}{L_Y^{(2)}}\right)}\int_{L_Y^{(1)}}^{L_Y^{(1)}+L_Y^{(2)}}f(Y)\\&\times\sin\left(\frac{n\pi(Y-L_Y^{(1)})}{L_Y^{(2)}}\right)dY,\end{aligned} \tag{2.35}$$

and

$$C_n^{(2)}=\frac{2}{L_Z\sinh\left(\frac{n\pi L_Y^{(2)}}{L_Z}\right)}\int_0^{L_Z}g(Z)\sin\left(\frac{n\pi Z}{L_Z}\right)dZ, \tag{2.36}$$

$$D_n^{(2)}=\frac{2}{L_Z\sinh\left(\frac{n\pi L_Y^{(2)}}{L_Z}\right)}\int_0^{L_Z}h(Z)\sin\left(\frac{n\pi Z}{L_Z}\right)dZ. \tag{2.37}$$

The solutions are symmetric about $Z = L_Z/2$. The aim is to obtain $f(Y)$ and $g(Z)$ for various prescribed top face displacements $h(Z)$. For a given $h(Z)$, $D_n^{(2)}$ can be calculated directly from Eq. (2.37). The other coefficients $A_n^{(1)}$, $B_n^{(1)}$, $D_n^{(1)}$ and $A_n^{(2)}$, $B_n^{(2)}$, $C_n^{(2)}$ can be solved via force, moment and displacement boundary conditions, at least numerically. The boundary conditions are the following:

(BC1) The nonlinear displacement u_2 is continuous across the interface,
(BC2) The nonlinear shear stress T_{xY}^{NL} is continuous across the interface,
(BC3) The nonlinear shear force associated with T_{xY} on the top and bottom faces is F_2,
(BC4) No net shear forces associated with T_{xZ} are applied on the Z-faces,
(BC5) The total moment about the Z-axis associated with T_{xZ} on the Z-faces is M_{xZ}.

The above five boundary conditions can be written mathematically as:

$$\text{(BC1)}\ u_2^{(1)}\left(Y=L_Y^{(1)}\right)=u_2^{(2)}\left(Y=L_Y^{(1)}\right). \tag{2.38}$$

$$\text{(BC2)}\ \mu_1\frac{\partial u_2^{(1)}(Y,Z)}{\partial Y}\bigg|_{Y=L_Y^{(1)}}=\mu_2\frac{\partial u_2^{(2)}(Y,Z)}{\partial Y}\bigg|_{Y=L_Y^{(1)}}, \tag{2.39}$$

$$\begin{aligned}\text{(BC3)}\ \int T_{xY}^{(1)NL}dXdZ&=F_2,\ \text{on } Y\\ &=0 \text{ and } \int T_{xY}^{(2)NL}dXdZ\\ &=F_2,\ \text{on } Y=L_Y^{(1)}+L_Y^{(2)}.\end{aligned} \tag{2.40}$$

$$\begin{aligned}\text{(BC4)}\ &\int_{Y=0}^{L_Y^{(1)}}\int_{X=0}^{L_X}T_{xZ}^{(1)}dXdY+\int_{Y=L_Y^{(1)}}^{L_Y^{(1)}+L_Y^{(2)}}\int_{X=0}^{L_X}T_{xZ}^{(2)}dXdY\\ &=0,\ \text{on } Z=0,L_Z.\end{aligned} \tag{2.41}$$

$$\begin{aligned}\text{(BC5)}\ &\int_{Y=0}^{L_Y^{(1)}}\int_{X=0}^{L_X}T_{xZ}^{(1)}(Z=0)YdXdY\\ &+\int_{Y=L_Y^{(1)}}^{L_Y^{(1)}+L_Y^{(2)}}\int_{X=0}^{L_X}T_{xZ}^{(2)}(Z=0)YdXdY,\\ &-\int_{Y=0}^{L_Y^{(1)}}\int_{X=0}^{L_X}T_{xZ}^{(1)}(Z=L_Z)YdXdY\\ &-\int_{Y=L_Y^{(1)}}^{L_Y^{(1)}+L_Y^{(2)}}\int_{X=0}^{L_X}T_{xZ}^{(2)}(Z=L_Z)YdXdY=M_{xZ}.\end{aligned} \tag{2.42}$$

From the first two boundary conditions, the following can be obtained:

$$\begin{aligned}&\sum_{n=1}^{\infty}D_n^{(1)}\sinh\frac{n\pi L_Y^{(1)}}{L_Z}\sin\frac{n\pi Z}{L_Z}\\ &=\sum_{n=1}^{\infty}C_n^{(2)}\sinh\frac{n\pi L_Y^{(2)}}{L_Z}\sin\frac{n\pi Z}{L_Z}\end{aligned} \tag{2.43}$$

and

$$\begin{aligned}&\sum_{n=1}^{\infty}n\pi\left(\mu_1L_Y^{(1)}L_Y^{(2)}D_n^{(1)}\cosh\frac{n\pi L_Y^{(1)}}{L_Z}\right.\\ &\left.+\mu_2L_Y^{(1)}L_Y^{(2)}C_n^{(2)}\cosh\frac{n\pi L_Y^{(2)}}{L_Z}-\mu_2L_Y^{(1)}L_Y^{(2)}D_n^{(2)}\right)\sin\frac{n\pi Z}{L_Z}\\ &=\sum_{n=1}^{\infty}n\pi L_Z\left(\mu_2L_Y^{(1)}A_n^{(2)}\left(\sinh\frac{n\pi(L_Z-Z)}{L_Y^{(2)}}+\sinh\frac{n\pi Z}{L_Y^{(2)}}\right)\right.\\ &\left.-(-1)^n\mu_1A_n^{(1)}L_Y^{(2)}\left(\sinh\frac{n\pi(L_Z-Z)}{L_Y^{(1)}}+\sinh\frac{n\pi Z}{L_Y^{(1)}}\right)\right).\end{aligned} \tag{2.44}$$

(BC3) can be written as:

$$\begin{aligned}&\sum_{n=1}^{\infty}\mu_1L_X(2A_n^{(1)}\left(\cosh\frac{n\pi L_Z}{L_Y^{(1)}}-1\right)+D_n^{(1)}(1-(-1)^n)\\ &=F_2,\ Y=0\end{aligned} \tag{2.45}$$

and

$$\begin{aligned}&\sum_{n=1}^{\infty}L_X\mu_2\left(2A_n^{(2)}(-1)^n\left(\cosh\frac{n\pi L_Z}{L_Y^{(2)}}-1\right)\right.\\ &\left.+D_n^{(2)}(1-(-1)^n)\cosh\frac{n\pi L_Y^{(2)}}{L_Z}+C_n^{(2)}(-1+(-1)^n)\right)\\ &=F_2,\ Y=L_Y^{(1)}+L_Y^{(2)}\end{aligned} \tag{2.46}$$

(BC4) can be written as:

$$\begin{aligned}&\sum_{n=1}^{\infty}\mu_1A_n^{(1)}(-1+(-1)^n)\left(\cosh\frac{n\pi L_Z}{L_Y^{(1)}}-1\right)\\ &+\mu_1D_n^{(1)}\left(\cosh\frac{n\pi L_Y^{(1)}}{L_Z}-1\right)\\ &+\mu_2A_n^{(2)}(-1+(-1)^n)\left(\cosh\frac{n\pi L_Z}{L_Y^{(2)}}-1\right)\\ &+\mu_2(C_n^{(2)}+D_n^{(2)})\left(\cosh\frac{n\pi L_Y^{(2)}}{L_Z}-1\right)=0\end{aligned} \tag{2.47}$$

and

$$\begin{aligned}&\sum_{n=1}^{\infty}-\mu_1A_n^{(1)}(-1+(-1)^n)\left(\cosh\frac{n\pi L_Z}{L_Y^{(1)}}-1\right)\\ &+\mu_1D_n^{(1)}(-1)^n\left(\cosh\frac{n\pi L_Y^{(1)}}{L_Z}-1\right)\\ &-\mu_2A_n^{(2)}(-1+(-1)^n)\left(\cosh\frac{n\pi L_Z}{L_Y^{(2)}}-1\right)\\ &+\mu_2(C_n^{(2)}+D_n^{(2)})(-1)^n\left(\cosh\frac{n\pi L_Y^{(2)}}{L_Z}-1\right)=0.\end{aligned} \tag{2.48}$$

The coefficients $A_n^{(1)}$, $B_n^{(1)}$, $D_n^{(1)}$ and $A_n^{(2)}$, $B_n^{(2)}$, $C_n^{(2)}$ should be determined using Eqs. (2.43)–(2.48). Finally, we note that the linear and nonlinear shear forces F_1 and F_2 cannot be measured separately. F_1 has been determined in terms of the imposed linear shear displacement δ_2, as shown in Eq. (2.25). It will be shown in the next section that F_2 can be determined in terms of M_{xZ} by (BC5), and thus F_1 and F_2 are both obtained in terms of the imposed quantities.

2.4. Particular problem

In this section, the solutions of the problem with $L_Y^{(1)}=L_Y^{(2)}$ are given analytically. This corresponds to the problem of a bilayer block with equal layer thicknesses. In addition, we consider the simple case of $h(Z)=0$. Based on the condition $L_Y^{(1)}=L_Y^{(2)}$, Eqs. (2.33) and (2.36) lead to:

$$D_n^{(1)}=C_n^{(2)}, \tag{2.49}$$

while Eq. (2.44) can be written as:

$$L_Y\sum_{n=1}^{\infty}\left(\left(\mu_1 D_n^{(1)}+\mu_2 C_n^{(2)}\right)\cosh\frac{n\pi L_Y}{L_Z}-\mu_2 D_n^{(2)}\right)\sin\frac{n\pi Z}{L_Z}$$
$$=L_Z\sum_{n=1}^{\infty}\left(\mu_2 A_n^{(2)}-(-1)^n\mu_1 A_n^{(1)}\right)\left(\sinh\frac{n\pi(L_Z-Z)}{L_Y}+\sinh\frac{n\pi Z}{L_Y}\right). \tag{2.50}$$

Since in Eq. (2.50),

$$\sin\frac{n\pi Z}{L_Z}\neq\sinh\frac{n\pi(L_Z-Z)}{L_Y}+\sinh\frac{n\pi Z}{L_Y}, \tag{2.51}$$

one possible set of solutions is such that each of the nth coefficients multiplying the sine and sinh terms is zero:

$$\left(\mu_1 D_n^{(1)}+\mu_2 C_n^{(2)}\right)\cosh\frac{n\pi L_Y}{L_Z}-\mu_2 D_n^{(2)}=0 \tag{2.52}$$

and

$$\mu_2 A_n^{(2)}-(-1)^n\mu_1 A_n^{(1)}=0. \tag{2.53}$$

Eqs. (2.47) and (2.48) can be written as:

$$\sum_{n=1}^{\infty}\mu_1 A_n^{(1)}(-1+(-1)^n)\left(\cosh\frac{n\pi L_Z}{L_Y}-1\right)$$
$$+\mu_1 D_n^{(1)}\left(\cosh\frac{n\pi L_Y}{L_Z}-1\right)$$
$$+\mu_2 A_n^{(2)}(-1+(-1)^n)\left(\cosh\frac{n\pi L_Z}{L_Y}-1\right)$$
$$+\mu_2\left(C_n^{(2)}+D_n^{(2)}\right)\left(\cosh\frac{n\pi L_Y}{L_Z}-1\right)=0, \tag{2.54}$$

and

$$\sum_{n=1}^{\infty}-\mu_1 A_n^{(1)}(-1+(-1)^n)\left(\cosh\frac{n\pi L_Z}{L_Y}-1\right)$$
$$+\mu_1 D_n^{(1)}(-1)^n\left(\cosh\frac{n\pi L_Y}{L_Z}-1\right)$$
$$-\mu_2 A_n^{(2)}(-1+(-1)^n)\left(\cosh\frac{n\pi L_Z}{L_Y}-1\right)$$
$$+\mu_2\left(C_n^{(2)}+D_n^{(2)}\right)(-1)^n\left(\cosh\frac{n\pi L_Y}{L_Z}-1\right)=0. \tag{2.55}$$

By adding and subtracting the above two equations, it can be shown that for each n:

$$\left(\mu_1 D_n^{(1)}+\mu_2 C_n^{(2)}+\mu_2 D_n^{(2)}\right)\left(\cosh\frac{n\pi L_Y}{L_Z}-1\right)=0. \tag{2.56}$$

Further, combining Eqs. (2.49), (2.52) and (2.56) leads to:

$$D_n^{(1)}=C_n^{(2)}=D_n^{(2)}=0. \tag{2.57}$$

By using Eq. (2.57), Eqs. (2.45) and (2.46) can be written as:

$$\sum_{n=1}^{\infty}2\mu_1 L_X A_n^{(1)}\left(\cosh\frac{n\pi L_Z}{L_Y}-1\right)=F_2, \tag{2.58}$$

$$\sum_{n=1}^{\infty}2\mu_2 L_X A_n^{(2)}(-1)^n\left(\cosh\frac{n\pi L_Z}{L_Y}-1\right)=F_2. \tag{2.59}$$

There are infinitely many coefficients $A_n^{(1)}$ and $A_n^{(2)}$ in the above two equations. However, experimental results show that the lateral profile $f(Y)$ of the block is approximated well by two half-period sine curves of different amplitudes. Hence, we choose $A_n^{(i)}=0$ for $n\geqslant 2$, and $A_1^{(1)}$ and $A_1^{(2)}$ can be solved from Eqs. (2.58) and (2.59) as:

$$A_1^{(1)}=\frac{F_2}{2\mu_1 L_X\left(\cosh\frac{\pi L_Z}{L_Y}-1\right)}, \tag{2.60}$$

$$A_1^{(2)}=-\frac{F_2}{2\mu_2 L_X\left(\cosh\frac{\pi L_Z}{L_Y}-1\right)}. \tag{2.61}$$

Finally, after integration (BC5) in Eq. (2.42) can be written as:

$$2\sum_{n=1}^{\infty}L_X L_Y\left(\cosh\frac{n\pi L_Z}{L_Y}-1\right)(-1)^n\left(\mu_1 A_n^{(1)}+\mu_2 A_n^{(2)}\right)$$
$$=M_{xZ}. \tag{2.62}$$

Substituting the solutions of $A_1^{(1)}$ and $A_1^{(2)}$ into the above equation, it can be obtained that

$$F_2=\frac{M_{xZ}}{2L_Y}. \tag{2.63}$$

With the coefficients $A_1^{(1)}$ and $A_1^{(2)}$ determined, the final form of $f(Y)$ according to Eqs. (2.29), (2.31) and (2.34) is thus:

$$f(Y)=A_1^{(1)}\sin\frac{\pi Y}{L_Y}\sinh\frac{\pi L_Z}{L_Y}, \tag{2.64}$$

for $0<Y<L_Y$, and

$$f(Y)=A_1^{(2)}\sin\frac{\pi(Y-L_Y)}{L_Y}\sinh\frac{\pi L_Z}{L_Y}. \tag{2.65}$$

for $L_Y<Y<2L_Y$. For later use, we further define the constants $a_1^{(1)}=A_1^{(1)}\sinh(\pi L_Z/L_Y)$ and $a_1^{(2)}=A_1^{(2)}\sinh(\pi L_Z/L_Y)$. By using Eq. (2.63), the total shear displacement in the composite block can be written as:

$$U^{(1)}(Y,Z)=\frac{\delta_2}{(1+\mu_1/\mu_2)L_Y}Y$$
$$+\frac{M_{xZ}}{4\mu_1 L_X L_Y\left(\cosh\frac{\pi L_Z}{L_Y}-1\right)}$$
$$\times\sin\frac{\pi Y}{L_Y}\left(\sinh\frac{\pi(L_Z-Z)}{L_Y}+\sinh\frac{\pi Z}{L_Y}\right), \tag{2.66}$$

for $0<Y<L_Y$, and

$$U^{(2)}(Y,Z)=\frac{\mu_2-\mu_1}{\mu_1+\mu_2}\delta_2+\frac{\delta_2}{(1+\mu_2/\mu_1)L_Y}Y$$
$$+\frac{M_{xZ}}{4\mu_2 L_X L_Y\left(\cosh\frac{\pi L_Z}{L_Y}-1\right)}$$
$$\times\sin\frac{\pi(Y-L_Y)}{L_Y}\left(\sinh\frac{\pi(L_Z-Z)}{L_Y}+\sinh\frac{\pi Z}{L_Y}\right), \tag{2.67}$$

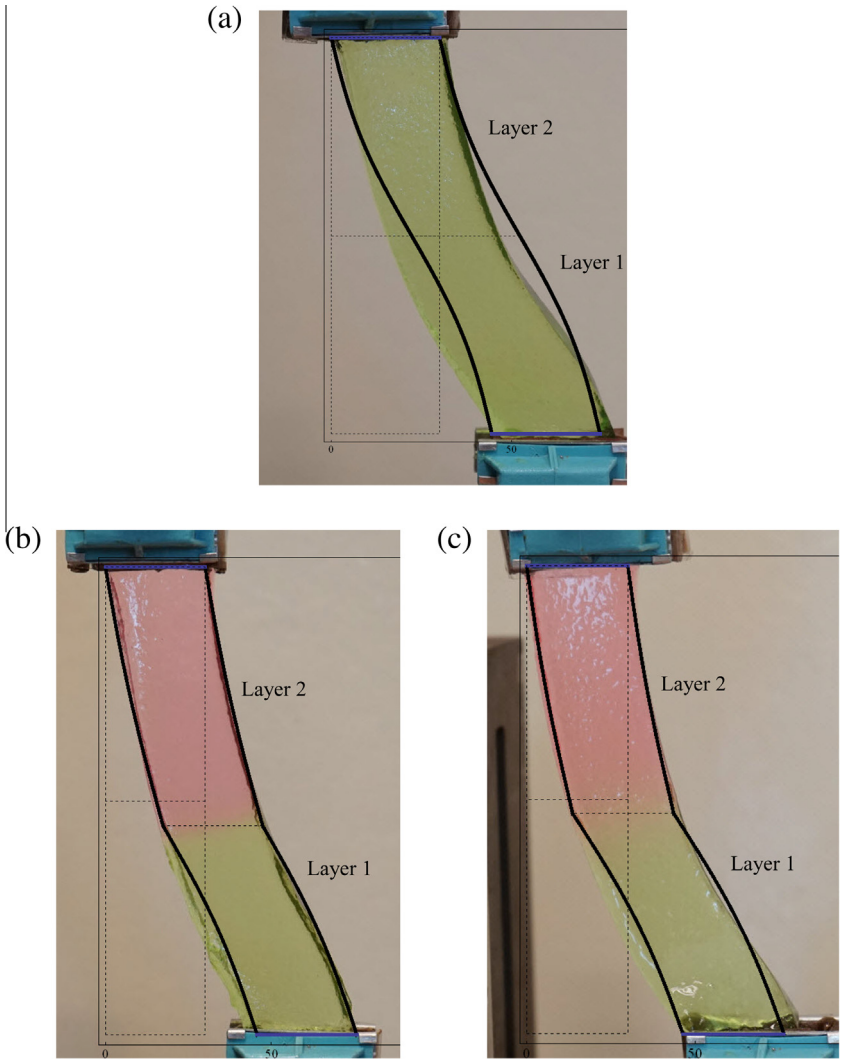

Fig. 2. Rectangular blocks of agar–gelatin gels, gripped at the top and subjected to a constant rightward shear displacement of 45 mm at the bottom. Layer 1 has the same stiffness, while Layer 2 is increasingly stiffer from (a) to (c). The theoretical lateral profiles are shown as solid lines.

for $L_Y < Y < 2L_Y$. In the above solutions, δ_2 is the prescribed linear displacement at the top face, and M_{xZ} is the prescribed moment about the Z-axis.

Eqs. (2.64)–(2.67) are explicit expressions for the lateral profile and the shear displacements in the composite block. The coefficients $A_1^{(1)}$ and $A_1^{(2)}$ may be estimated from the experimental data for the lateral profile of the block. Knowing these two values, the predicted and experimental profiles can be compared. Similarly, coefficients such as M_{xZ}/μ_1 and M_{xZ}/μ_2 can be determined to be $4A_1^{(1)}L_XL_Y(\cosh\pi L_Z/L_Y - 1)$ and $-4A_1^{(2)}L_XL_Y(\cosh\pi L_Z/L_Y - 1)$, respectively. Hence, the shear displacements can also be computed based on the experimental data.

3. Experimental and numerical results

In this section, experimental results on bilayer blocks of an agar–gelatin are reported and compared to the theoretical predictions. Following this, the dependence of the second-order nonlinear effects on the elastic dissimilarity, i.e., the normal stresses and the out-of-plane shear stress, as well as the interfacial displacement in the vertical direction, is studied.

3.1. Theoretical and experimental profiles of sheared bilayer blocks

Bilayer blocks with the dimensions $L_X = 30$ mm, $L_Y^{(1)} = L_Y^{(2)} = 70$ mm and $L_Z = 25$ mm were made from an agar–gelatin. In Fig. 2(a–c), Layer 1 (lower layer) has a concentration of 17 g of the gelatin powder in 110 mL of water, while Layer 2 (upper layer) has the concentrations of 17 g/110 mL, 17 g/100 mL and 17 g/90 mL, respectively. Thus, the block in Fig. 2(a) is homogeneous, and the upper layers are stiffer than the lower layers in the other two blocks. The bottom faces of all three blocks were sheared towards the right by a distance of 45 mm.

Table 1
Parameters used in Fig. 2.

	Fig. 2(a)	Fig. 2(b)	Fig. 2(c)
Samples			
Layer 1 concentration	17 g/110 mL water	17 g/110 mL water	17 g/110 mL water
Layer 2 concentration	17 g/110 mL water	17 g/100 mL water	17 g/90 mL water
L_X	30 mm	30 mm	30 mm
$L_Y^{(1)}$	70 mm	70 mm	70 mm
$L_Y^{(2)}$	70 mm	70 mm	70 mm
L_Z	25 mm	25 mm	25 mm
Applied shear displacement			
δ_2	45 mm	45 mm	45 mm
Parameters estimated from experiments			
$a_1^{(1)}$	3 mm	3 mm	2.5 mm
$a_1^{(2)}$	3 mm	1.48 mm	0.925 mm

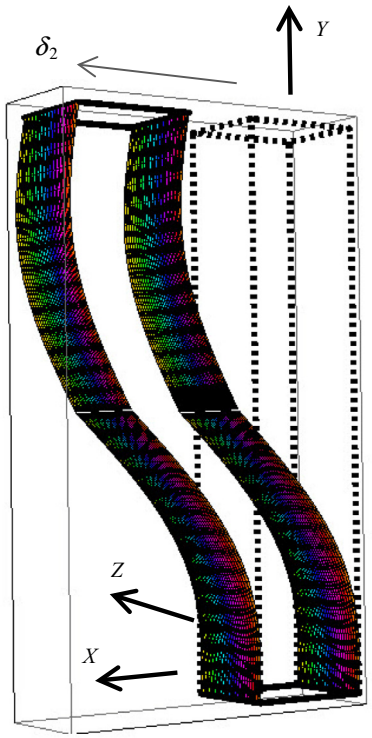

Fig. 3. Deformed and undeformed states of a bilayer rectangular block under generalized shear. The prescribed shear displacement $\delta_2 = 0.045$ m at the top and the prescribed moment $M_{xZ} = -0.42$ N · m.

The experimental lateral profiles $f(Y)$ are curved; they are not a linear function of Y. The homogeneous block displays a smooth curved profile. In the deformed bilayers, each block has a smooth profile but they also have a discernible kink at the interface. Comparing the slopes $f'(Y)$ of the upper blocks just above the interface, it can be seen that the stiffest block in Fig. 2(c) has the smallest slope. Just below the interface, the lower block in Fig. 2(c) appears to have a larger slope. These observations agree with intuition, since the stiffest upper block will deform the least and the corresponding lower block will deform more at the connecting interface to compensate for the smaller deformation of the upper block. The theoretical profiles, which consist of a sine curve superimposed on a straight line, are highlighted in bold. Table 1 shows the values of the parameters α_1, α_2, $a_1^{(1)}$ and $a_1^{(2)}$ used to generate these profiles. The theoretical profiles capture the essential features described above (kinks and the slopes at the interface). Discrepancy between the theoretical and observed profiles is also evident, notably the greater sagging of the experimental samples. This could be attributed to gravity effects and the limitations of a second-order nonlinear elasticity model.

In Fig. 3, the three-dimensional profile of an entire deformed bilayer block is simulated for a specific set of elastic constants, prescribed displacement of 0.045 m and prescribed moment of −0.42 N · m, as listed in Table 2. This shows more clearly how the $X = 0$ and $X = L_X$ surfaces deform from their original positions resulting in unequally curved faces meeting at a kink at the interface, as well as the maintenance of the boundary conditions (fixed base, constant total height).

Table 2
Elastic parameters used in Figs. 3–8. The unit of elastic constants is kPa. The dimensions of the block are $L_X = 0.030$ m, $L_Y^{(1)} = L_Y^{(2)} = 0.070$ m, $L_Z = 0.025$ m. Also, $\delta_2 = 0.045$ m in all figures, while $M_{xZ} = -0.42$ N · m in Fig. 3 and −014 N · m in Figs. 4–8.

	λ_1 λ_2	μ_1 μ_2	m_1 m_2	n_1 n_2
Fig 3	2.25×10^6	8	-20×10^6	−80
	60	12.21	−35.60	−23.50
Fig. 4	1024		−2400	−2350
	1024		−2400	−2350
Fig. 5	357		−1000	−235
		103	−1000	−235
Fig. 6(a)	3570		−8465	−2350
	3570	103000		−2350
Fig. 6(b)	3570		−2394	−2350
	3570	103000		−2350
Fig. 7	2.25×10^6	8	-20×10^6	−80
	60	21.62	−35.60	−23.50
Fig. 8(a)	1×10^8	100	-2×10^8	−800
	1×10^8			−800
Fig. 8(b)	1×10^8		-2×10^8	−800
	1×10^8		-2×10^8	−800

3.2. Dependence of second-order stresses on elastic inhomogeneity

In this section, the dependence of the second-order normal stresses on the layer elastic inhomogeneity (dissimilarity in the elastic constants) is studied. Three types of inhomogeneity are considered: dissimilarity in one particular constant, e.g., μ_1/μ_2, dissimilarity between constants of the same order, e.g., λ_2/μ_1, and dissimilarity between constants of different orders, e.g., m_2/μ_1. In all the figures to follow, $\delta_2 = 0.045$ m and $M_{xZ} = -0.14$ N · m.

3.2.1. Inhomogeneity of shear moduli

Fig. 4(a–c) plot $T^{(1)}_{xX}$, $T^{(1)}_{yY}$ and $T^{(1)}_{zZ}$ in Layer 1, respectively, versus the shear modulus μ_2 of Layer 2 for various constant values of $\mu_1/\mu_2 = 0.1$, 0.4, 1, 2.5 and 10. All other elastic constants are held constant and are the same between the layers, as shown in Table 2. The applied boundary conditions are also indicated in this table. The ratio $\mu_1/\mu_2 = 1$ implies a homogeneous block. Although the normal stresses are constant in each layer of the block, they, except for $T^{(1)}_{yY}$, will generally have a jump across the interface, i.e., $T^{(1)}_{xX} \neq T^{(2)}_{xX}$, $T^{(1)}_{zZ} \neq T^{(2)}_{zZ}$ but $T^{(1)}_{yY} = T^{(2)}_{yY}$.

This figure shows a rich behavior of the stresses. First, the dependence on inhomogeneity is clearly seen, and is generally significant. Changing μ_1/μ_2 from 1 to 0.1 at $\mu_2 = 200$ kPa increases $T^{(1)}_{xX}$ significantly from ~ -60 to ~ -135 kPa, for instance.

Second, within the range of μ_2 studied and depending on μ_1/μ_2, the stresses can either increase or decrease monotonically, or they might have extrema. This highlights the complexity and hence difficulty of materials selection if the aim is to minimize or maximize the normal stresses.

Third, the stresses can be either zero, positive or negative. $T^{(1)}_{xX}$ and $T^{(1)}_{yY}$ appear to be mostly compressive except at large μ_2, whereas $T^{(1)}_{zZ}$ is largely tensile if the lower layer is more compliant then the upper layer ($\mu_1/\mu_2 < 1$). These stresses, in particular $T^{(1)}_{zZ}$, demonstrate the Poynting effect under shear. This corresponds to the extension or contraction of a twisted rod in the direction perpendicular to the plane of shearing. The second-order stresses are necessary to maintain the deformation of the generalized shear. In the absence of a positive (negative) $T^{(1)}_{zZ}$, the block will contract (expand) along the Z-direction, corresponding to a negative (positive) Poynting effect. Because $T^{(1)}_{zZ} \neq T^{(2)}_{zZ}$, there is a tendency for the bilayer block to contract or expand by different amounts.

Fourth, it is difficult to generalize whether the magnitude of the stresses will increase or decrease if the lower layer becomes more compliant compared to the upper layer. Nevertheless, some general trend can still be observed. Consider Fig. 4(b) for μ_2 held fixed at 1000 kPa. If the block is homogeneous, $T^{(1)}_{yY}$ is slightly tensile ($\sim$25 kPa). If Layer 1 becomes more compliant relative to Layer 2, $T^{(1)}_{yY}$ becomes more compressive, with $T^{(1)}_{yY} \sim -140$ kPa when $\mu_1/\mu_2 = 0.1$. If Layer 1 becomes stiffer, $T^{(1)}_{yY}$ becomes more tensile, with $T^{(1)}_{yY} \sim 100$ kPa when $\mu_1/\mu_2 = 10$.

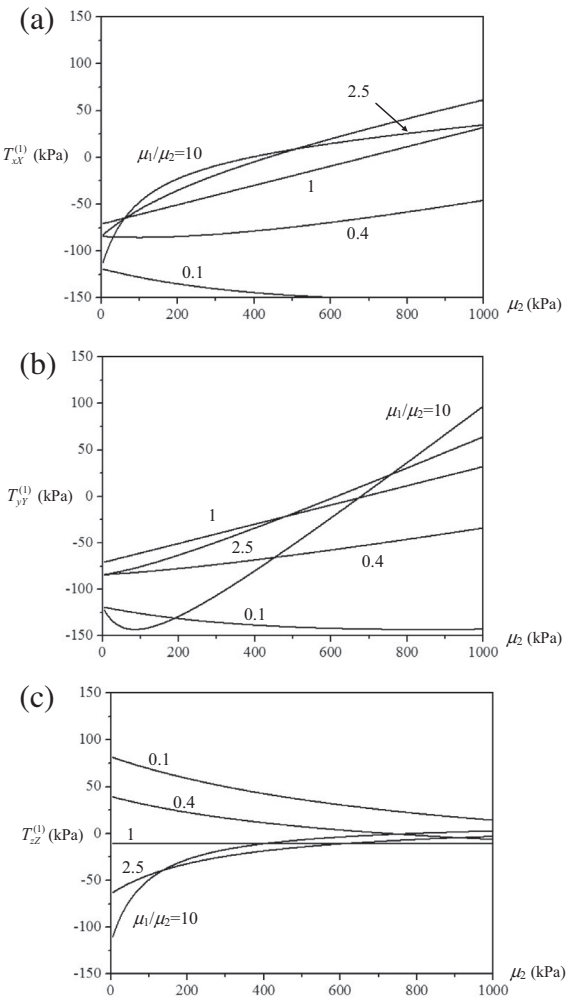

Fig. 4. Dependence of the stresses (a) $T^{(1)}_{xX}$, (b) $T^{(1)}_{yY}$ and (c) $T^{(1)}_{zZ}$ in Layer 1 with μ_2 for inhomogeneity ratios $\mu_1/\mu_2 = 0.1$, 0.4, 1, 2.5, 10. The other elastic constants are listed in Table 2. The influence of the ratios on the stresses is extrinsic, i.e., it persists even as μ_2 tends to zero.

Fifth, it is interesting that $T^{(1)}_{yY}$ remains the same if the materials are interchanged across the layers, as can be verified using Fig. 4(b). For instance, if $\mu_2 = 500$ kPa and $\mu_1 = 200$ kPa, and if $\mu_2 = 200$ kPa and $\mu_1 = 500$ kPa, $T^{(1)}_{yY} \sim -63$ kPa in both cases. This is related to the requirement of the continuity of T_{yY} across the interface. The same does not hold for the other normal stress components, as they experience a jump in value across the interface.

Sixth, each normal stress generally tends to different values as μ_2 tends to zero, depending on the ratio μ_1/μ_2. Although both μ_1 and μ_2 approach zero, the induced normal stresses can be very different if μ_1 approaches zero faster or slower than μ_2. Indeed, Fig. 4(c) shows that when μ_2 tends to zero, $T^{(1)}_{zZ}$ is $\sim$80 kPa if μ_1 is ten times smaller than μ_2, while $T^{(1)}_{zZ}$ is ~ -110 kPa if μ_1 is ten times larger. This suggests the intrinsic importance of elastic inhomogeneity: it may significantly influence the magnitude and sign of the second-order stresses even though the individual constants are themselves vanishingly small. However, exceptions do occur in the case of $T^{(1)}_{xX}$ and $T^{(1)}_{yY}$: if two ratios of μ_1/μ_2 are

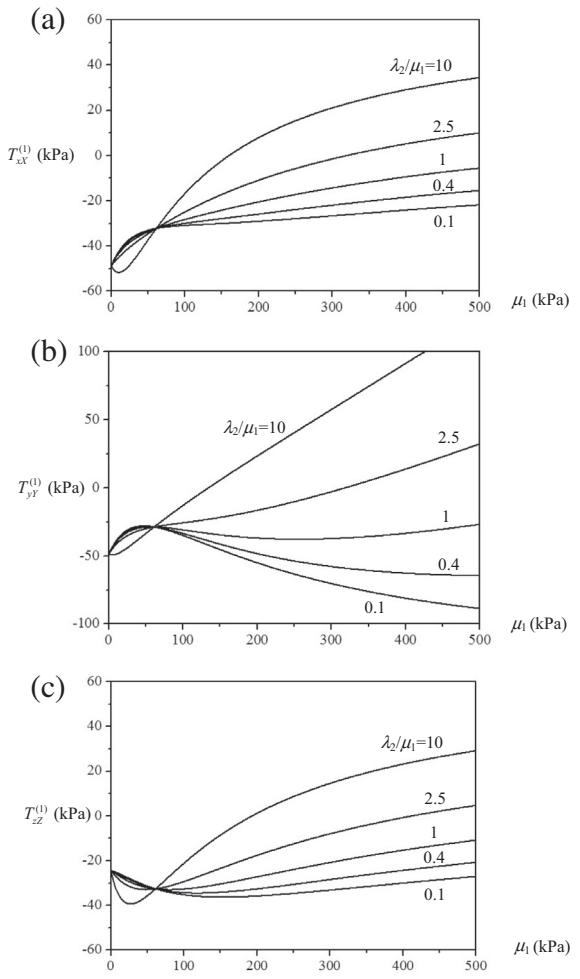

Fig. 5. Dependence of the stresses (a) $T^{(1)}_{xX}$, (b) $T^{(1)}_{yY}$ and (c) $T^{(1)}_{zZ}$ in Layer 1 with μ_1 for inhomogeneity ratios λ_2/μ_1 = 0.1, 0.4, 1, 2.5, 10. The other elastic constants are listed in Table 2. The influence of the ratios on the stresses is intrinsic, i.e., it does not persist as μ_1 tends to zero.

reciprocals of each other, these two stresses do tend to the same values when μ_1 and μ_2 approach zero. This can be seen in Fig. 4(a) and (b) where the curves for μ_1/μ_2 = 10 and 0.1 (or 2.5 and 0.4) meet each other at μ_2 = 0.

3.2.2. Inhomogeneity of Lamé constants

Next, the dependence of $T^{(1)}_{xX}$, $T^{(1)}_{yY}$ and $T^{(1)}_{zZ}$ on μ_1 for λ_2/μ_1 = 0.1, 0.4, 1, 2.5 and 10 is studied. All other elastic constants and the prescribed boundary conditions are given in Table 2. Note that $\lambda_2/\mu_1 = 1$ does not imply a homogeneous block. The results are shown in Fig. 5. The *Lamé* first constant λ_2 is related to the Poisson ratio ν_2 and shear modulus μ_2 (all of Layer 2) according to $\nu_2 = 1/2(1 + \mu_2/\lambda_2)$. Hence for a fixed μ_2, as is the case here, increasing λ_2 implies that ν_2 approaches 0.5, i.e., Layer 2 tends towards incompressibility.

The dependence of all three normal stresses on μ_1 appears to be similar. Many of the remarks made with regard to Fig. 4 also hold here: the dependence on the inhomogeneity is significant, the stresses can vary monotonically with μ_1 or possess extrema, depending on

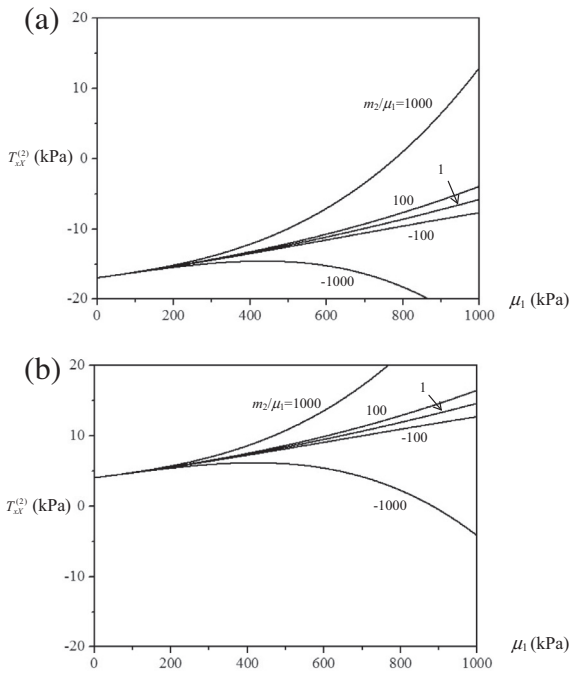

Fig. 6. Dependence of the stress $T^{(2)}_{xX}$ in Layer 2 with μ_1 for m_2/μ_1 = −1000, −100, 1, 100 and 1000. In (a) m_1 = −8465 kPa; in (b) m_1 = −2394 kPa. The other elastic constants are listed in Table 2. For the most part, changing the value of m_1 results in a change in the sign of the stress.

λ_2/μ_1, and they can either demonstrate the positive or negative Poynting effect. An important result of Fig. 5 is that the Poynting effect becomes more significant (the normal stresses increase in magnitude) as Layer 2 approaches incompressibility. For the elastic constants considered here, these normal stresses are tensile at large values of λ_2/μ_1, i.e., the bilayer block tends to demonstrate a negative Poynting effect. A further interesting feature of the curves in Fig. 5 is that there appears to be a specific combination of the elastic constants that yields identical values of the stresses. This congruence of stress values occurs at $\mu_1 \sim 61$ kPa, regardless of the value of λ_2. This can be understood from Eq. (2.20), where $C^{(1)}_3$ (which essentially determines the normal stresses) can be expressed in the form of $\gamma_1(\gamma_2 + \gamma_3\lambda_2)/(\gamma_2 + \gamma_3\lambda_2)$, where γ_1, γ_2 and γ_3 are some combinations of elastic constants, which leads to the cancelation of the common factor in the numerator and denominator and hence elimination of λ_2 from the stress dependence.

Note also that as μ_1 tends to zero, each normal stress converges to a single negative value irrespective of λ_2/μ_1. This is unlike the results in Fig. 4. This means that as long as both μ_1 and λ_2 approach zero, each induced normal stress will be independent of how fast λ_2 approaches zero relative to μ_1.

3.2.3. Inhomogeneity of second- and third-order elastic constants

Fig. 6 plots the variation of $T^{(2)}_{xX}$ in Layer 2 with μ_1 of Layer 1 for m_2/μ_1 = −1000, −100, 1, 100, and 1000. The value of

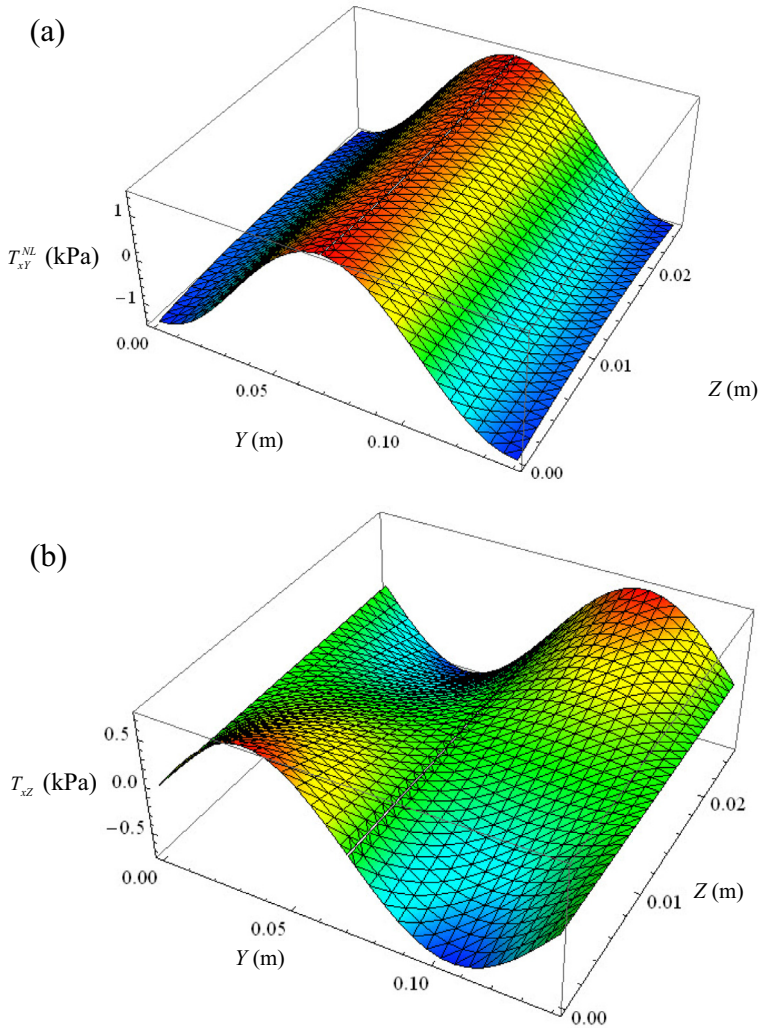

Fig. 7. Dependence of the second-order shear stresses (a) T_{xY}^{NL} and (b) T_{xZ} on the Y and Z coordinates of a bilayer rectangular block under generalized shear. The sinusoidally varying T_{xZ} gives rise to a generalized Poynting effect.

$m_1 = -8465$ and -2394 kPa in Fig. 6(a) and (b), respectively. Other relevant parameters are given in Table 2.

Overall, it can be observed that changing the value of m_1 results in a change in the sign of the stress. Similar to Fig. 5, a notable result of Fig. 6 is the convergence of $T_{xX}^{(2)}$ as the Layer 1 shear modulus tends to zero. When the shear modulus of Layer 1 becomes vanishingly smaller, it appears that changing the other elastic constants of Layer 2 (λ_2 and m_2) will not alter the induced normal stresses. However, the values of these stresses would depend on the particular elastic constants. In Fig. 6, $T_{xX}^{(2)}$ tends to ~ -17 and ~ 4 kPa for $m_1 = -8465$ and -2394 kPa, respectively.

Taking Figs. 4–6 together, we observe an important effect of layer elastic inhomogeneity. If the inhomogeneity is between the shear moduli μ_1/μ_2, then its influence on the normal stresses is intrinsic, meaning that the stresses may differ in magnitude and sign if these ratios are different, even if the actual values of the individual constants are vanishingly small. Exception does occur for $T_{xX}^{(1)}$ and $T_{yY}^{(1)}$ when the values of μ_1/μ_2 are reciprocals of each other. If the inhomogeneity is between other types of elastic constants, such as λ_2/μ_1 and m_2/μ_1, each normal stress will be influenced by this inhomogeneity ratio only when the elastic constants themselves are not vanishingly small. This may be termed an extrinsic influence, in the sense that the inhomogeneity ratio has an effect only when the individual constants are not vanishingly small. Further simulations show that all other inhomogeneity ratios such as λ_1/λ_2, m_1/m_2, n_1/n_2, λ_1/μ_2, m_1/μ_2, m_2/λ_1 and m_1/λ_2 exert an extrinsic influence on the normal stresses.

3.2.4. Variation of the second-order shear stresses in the vertical plane

To illustrate how the second-order shear stresses vary in the block, T_{xY}^{NL} and T_{xZ} are plotted versus Y and Z for the set of elastic constants and boundary conditions given in Table 2. These stresses are not a function of X.

Both shear stresses are of the order of 1 kPa and are not small compared to the shear moduli $\mu_1 = 8$ kPa and $\mu_2 = 21.62$ kPa. T_{xY}^{NL} reaches its maximum at mid-height

and does not vary too much with Z. The distribution of T_{xZ} in Fig. 7(b) is more complex than that of T_{xY}^{NL} in Fig. 7(a). First, T_{xZ} is a strong function of both Y and Z. Second, the distribution is odd with respect to Y and Z. Thus, with respect to the mid-height position, T_{xZ} ($Y = 0.05$ m, Z) and T_{xZ} ($Y = 0.1$ m, Z) have different signs. The signs of these stresses are also reversed with respect to the mid-position of Z.

We further note that T_{xZ} is not present in simple shear when the shear displacement U is taken to be a function of Y only. In generalized shear when U is a function of both Y and Z, T_{xZ} exists and tends to distort the block about the Y-axis. Thus, a block when sheared only in the X-direction (shearing of the block in the X–Y plane about the Z-direction) may also tend to shear in the out-of-plane Z-direction (shearing in the X–Z plane about the Y-direction). This effect may be called a generalized Poynting effect, in analogy with the existence of the normal stresses under simple shear. A similar terminology has been given by dell'Isola et al. (1998), in which a bar when bent stretches in the absence of second-order resultant normal force.

3.2.5. Dependence of the interface vertical displacement on elastic constants

According to Eq. (2.15), vertical displacements exist in the bilayer block. In Fig. 8, $V = v_1\left(Y = L_Y^{(1)}\right) + v_2\left(Y = L_Y^{(1)}\right)$ at the interface versus the change in elastic constants is investigated. Fig. 8(a) plots V versus μ_2 for $m_2 = 0, \pm 1.5 \times 10^8, \pm 3 \times 10^7$ kPa, while Fig. 8(b) plots V versus μ_1 for $\mu_2 = 10, 30, 50, 100, 300$ kPa. Other parameters are given in Table 2.

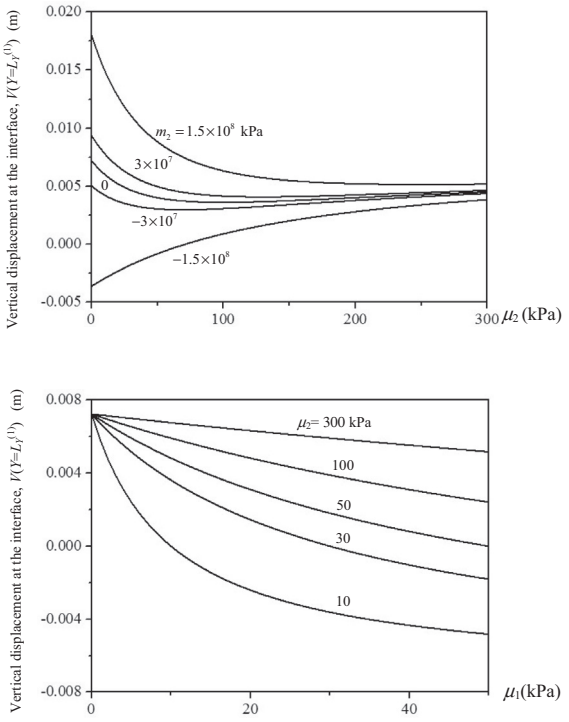

Fig. 8. Dependence of the vertical displacement at the interface $V(Y = L_Y^{(1)})$ on (a) μ_2 for different values of m_2 between -1.5×10^8 and 1.5×10^8 kPa, and (b) μ_1 for different values of μ_2 between 10 and 300 kPa. Strong influence of elastic inhomogeneity on the displacement is evident.

These interfacial displacements are of the order of 0.01 m, a significant fraction of the height (0.14 m) of the block in this simulation. The interface can either migrate upwards or downwards depending on the combination of elastic constants. For a homogeneous block, there will be no interfacial displacement. Hence, the interfaces in bilayer devices may be designed to move in one direction or another through a judicious selection of the layer materials.

The limiting behavior of the interfacial displacement when μ_2 and μ_1 tend to zero in Fig. 8(a) and (b), respectively, is interesting. Fig. 8(a) shows that varying m_2 leads to different values of V in the limit $\mu_2 \to 0$, while Fig. 8(b) shows that V is independent of μ_2 in the limit $\mu_1 \to 0$. The results in this figure show that it is possible to control the interfacial displacement using either a second- or a third-order elastic constant.

4. Conclusions

In this paper, the generalized shear of a soft bilayer block is investigated using second-order elasticity. The key contributions are (i) the study of a bilayer block, in contrast to homogeneous blocks studied in most previous works, (ii) a more general assumption of the shear displacement being a function of Y and Z rather than Y alone, and (iii) verification of theoretical predictions with experiments.

In the experiments, agar–gelatin bilayer blocks deformed under shear display lateral profiles which are in good agreement with the theoretical predictions. The presence of smooth profiles of different curvatures meeting at a kink at the interface is predicted.

The numerical simulations, focusing on the dependence of the second-order effects on the elastic constants, lead to the following conclusions: (i) the layer elasticity inhomogeneity can influence significantly the sign and the magnitude of the second-order normal and shear stresses as well as the interfacial displacement, (ii) the inhomogeneity as represented by the ratio of the shear moduli has an intrinsic influence on the stresses, while inhomogeneity between all other constants has an extrinsic influence, (iii) the Poynting effect is predicted for both homogeneous and bilayer blocks, and (iv) a generalized Poynting effect is also evident, in which an out-of-plane shear stress is induced when the block is sheared in-plane.

References

Butler, P.J., Norwich, G., Weinbaum, S., Chien, S., 2001. Shear stress induces a time- and position-dependent increase in endothelial cell membrane fluidity. Am. J. Physiol.-Cell Physiol. 280, C962–C969.

Cadelano, E., Palla, P.L., Giordano, S., Colombo, L., 2009. Nonlinear elasticity of monolayer graphene. Phys. Rev. Lett. 102, 235502.

Dell'Isola, F., Ruta, G.C., Batra, R.C., 1998. Generalized Poynting effects in predeformed prismatic bars. J. Elast. 50, 181–196.

Destrade, M., Murphy, J.G., Saccomandi, G., 2012. Simple shear is not so simple. Int. J. Nonlinear Mech. 47, 210–214.

Destrade, M., Saccomandi, G., 2010. On the rectilinear shear of compressible and incompressible elastic slabs. Int. J. Eng. Sci. 48, 1202–1211.
Horgan, C.O., Murphy, J.G., 2011. Simple shearing of soft biological tissues. Proc. R. Soc. A – Math. Phys. 467, 760–777.
Janmey, P.A., Mccormick, M.E., Rammensee, S., Leight, J.L., Georges, P.C., Mackintosh, F.C., 2007. Negative normal stress in semiflexible biopolymer gels. Nat. Mater. 6, 48–51.
Jönsson, P., Beech, J.P., Tegenfeldt, J.O., Hook, F., 2009. Mechanical behavior of a supported lipid bilayer under external shear forces. Langmuir 25, 6279–6286.
Kang, H., Wen, Q., Janmey, P.A., Tang, J.X., Conti, E., MacKintosh, F.C., 2009. Nonlinear elasticity of stiff filament networks: strain stiffening, negative normal stress, and filament alignment in fibrin gels. J. Phys. Chem. B 113, 3799–3805.
Lu, Q., Huang, R., 2009. Nonlinear mechanics of single-atomic-layer graphene sheets. Int. J. Appl. Mech. 1, 443–467.
Mihai, L.A., Goriely, A., 2013. Numerical simulation of shear and the Poynting effects by the finite element method: an application of the generalised empirical inequalities in non-linear elasticity. Int. J. Nonlinear Mech. 49, 1–14.
Murnaghan, F.D., 1951. Finite Deformation of an Elastic Solid. John Wiley, New York.
Peng, Z.L., Li, X.J., Pivkin, I.V., Dao, M., Karniadakis, G.E., Suresh, S., 2013. Lipid bilayer and cytoskeletal interactions in a red blood cell. Proc. Natl. Acad. Sci. USA 110, 13356–13361.
Scarpa, F., Adhikari, S., Chowdhury, R., 2010. The transverse elasticity of bilayer graphene. Phys. Lett. A 374, 2053–2057.
Storm, C., Pastore, J.J., MacKintosh, F.C., Lubensky, T.C., Janmey, P.A., 2005. Nonlinear elasticity in biological gels. Nature 435, 191–194.
Wang, D., Wu, M.S., 2014a. Generalized shear of a soft rectangular block. J. Mech. Phys. Solids 70, 297–313.
Wang, D., Wu, M.S., 2014b. Poynting and axial force-twist effects in nonlinear elastic mono- and bi-layered cylinders: torsion, axial and combined loadings. Int. J. Solids Struct. 51, 1003–1019.
Wu, M.S., Kirchner, H.O.K., 2010. Nonlinear elasticity modeling of biogels. J. Mech. Phys. Solids 58, 300–310.